NANO LETTERS

pubs.acs.org/NanoLett Letter

Quantized Exciton Motion and Fine Energy-Level Structure of a Single Perovskite Nanowire

Ying Tang,[#] Chunyang Yin,[#] Qiang Jing,[#] Chunfeng Zhang, Zhi-Gang Yu,* Zhenda Lu,* Min Xiao,* and Xiaoyong Wang*

Cite This: *Nano Lett.* 2022, 22, 2907−2914 Read Online

ACCESS | Metrics & More | Article Recommendations | Supporting Information

ABSTRACT: The quantum-confinement effect profoundly influences the exciton energy-level structures and recombination dynamics of semiconductor nanostructures but remains largely unexplored in traditional one-dimensional nanowires mainly due to their poor optical qualities. Here, we show that in defect-tolerant perovskite material of highly luminescent $CsPbBr_3$ nanowires, the exciton's center-of-mass motion perpendicular to the axial direction is severely confined. This is reflected in the two sets of photoluminescence spectra emitted from a single $CsPbBr_3$ nanowire, each of which consists of doublet peaks with linear polarizations perpendicular and parallel to the axial direction. Moreover, different exciton states can be mixed by the Rashba spin−orbit coupling effect, resulting in two single photoluminescence peaks with linear polarizations both along the nanowire axis. The above findings mark the emergence of an ideal platform for the exploration of intrinsic one-dimensional exciton photophysics and optoelectronics, thus bridging the long-missing research gap between the well-studied two- and zero-dimensional semiconductor nanostructures.

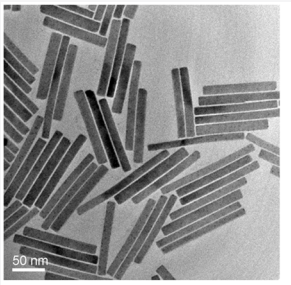

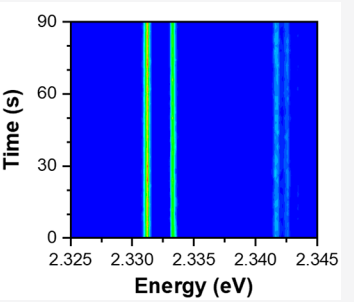

KEYWORDS: *perovskite, $CsPbBr_3$, nanowire, quantized exciton motion, fine energy-level structure*

INTRODUCTION

In low-dimensional semiconductors of nanorods (NRs) and nanowires (NWRs), the exciton motion along the axial direction is essentially uninhibited whereas that in the perpendicular direction is severely confined. Novel behaviors of exciton generation, recombination, and transport, which are critical for the efficient operations of relevant solar-cell and photodetector devices,[1] are thus anticipated from these one-dimensional (1D) NRs and NWRs.[2] In the model material system of colloidal CdSe, various optical and electronic properties have already been revealed from the NR structures, which are significantly different from those of their counterpart zero-dimensional (0D) quantum dots (QDs). These mainly include but are not limited to linearly polarized emission along the axial direction,[3] symmetry crossing between the bright- and dark-exciton states,[4] transition from three- to two-particle Auger recombination,[5] and ease in manipulating the overlap of electron−hole wave functions by external electric fields.[6]

When the rod length is further increased to surpass several tens of nanometers, the as-formed CdSe NWRs are normally associated with rampant defect sites to cause a significant reduction of photoluminescence (PL) efficiencies.[7−9] Consequently, the 1D exciton features were vaguely observed only in a limited number of previous optical studies, such as synchronous PL blinking[8] and efficient carrier transport[10] spanning the entire length of a single CdSe NWR. Similar issues of high defect concentrations and low PL efficiencies have also plagued the single-walled carbon nanotubes (SWCNTs),[11,12] whose 1D exciton feature is mainly reflected in the exciton−exciton annihilation effect.[13,14] While recent breakthroughs in material processing have promoted single-photon emission from individual SWCNTs with superior PL characteristics,[15] the quasi-1D motion of excitons is inevitably lost due to the formation of localized states.[16−18] As such, the exciton photophysics of 1D semiconductor NWRs remains largely unexplored up to now. More appropriate material systems, such as the newly emerged perovskite nanocrystals with a strong defect-tolerance feature,[19,20] are thus needed to fulfill this challenging goal.

Here, we have synthesized highly luminescent perovskite $CsPbBr_3$ NWRs and characterized their single-particle optical properties mainly at the cryogenic temperature. A single NWR can emit one set of doublet PL peaks with linear polarizations perpendicular and parallel to the axial direction, respectively, which are reminiscent of the fine energy-level structures of *X*

Received: January 7, 2022
Revised: March 22, 2022
Published: April 1, 2022

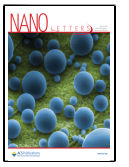

https://doi.org/10.1021/acs.nanolett.2c00079
Nano Lett. 2022, 22, 2907−2914

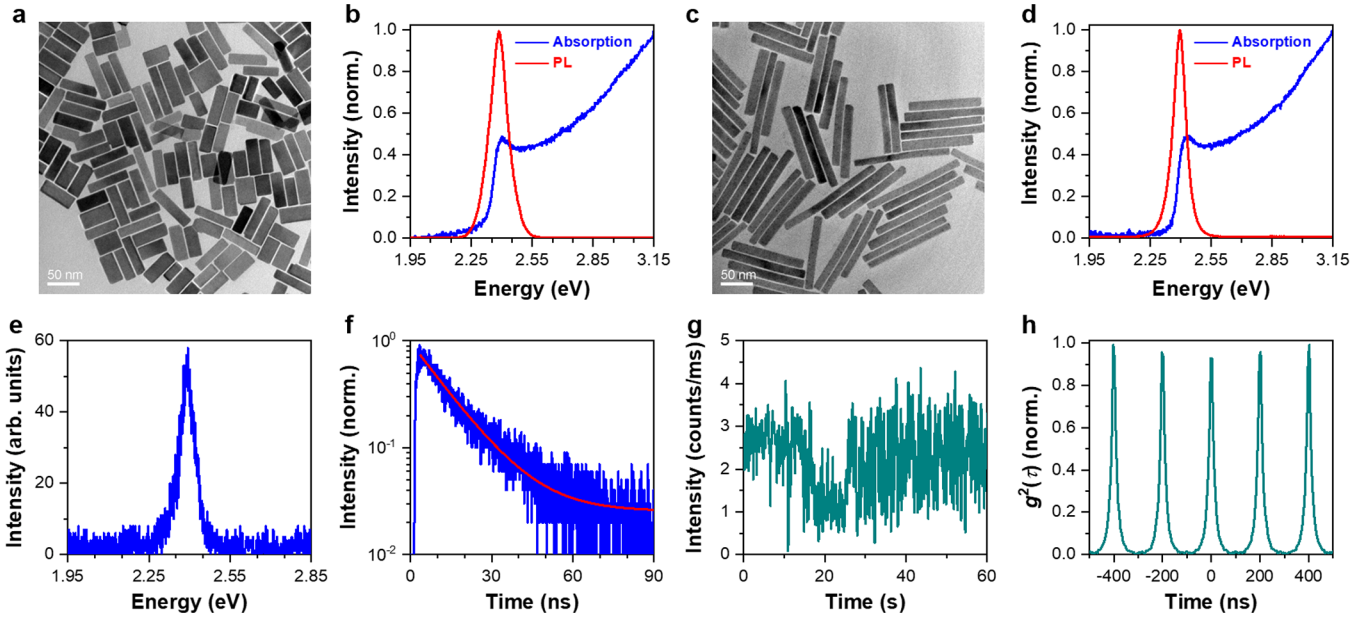

Figure 1. Structural and optical characterizations at room temperature. (a) Transmission electron microscopy image of $CsPbBr_3$ SNWRs. (b) Solution absorption and PL spectra of $CsPbBr_3$ SNWRs. (c) Transmission electron microscopy image of $CsPbBr_3$ LNWRs. (d) Solution absorption and PL spectra of $CsPbBr_3$ LNWRs. (e) PL spectrum of a single $CsPbBr_3$ SNWR. (f) PL decay curve of a single $CsPbBr_3$ SNWR fitted with the single-exponential lifetime of ~8.26 ns. (g) PL intensity time trace of a single $CsPbBr_3$ SNWR plotted with a binning time of 100 ms. (h) Second-order photon correlation measurement of a single $CsPbBr_3$ SNWR with the $g^{(2)}(0)$ value of ~0.93.

and Z excitons commonly observed in its counterpart 0D QDs. Surprisingly, two sets of such doublet PL peaks can be simultaneously observed in a single NWR, whose central-energy separation is much larger than the exciton fine-structure splitting due to long- and short-range exchange interactions. We show that they are caused by the quantized motion of X and Z excitons perpendicular to the axial direction of a single NWR. In addition, some of the single NWRs exhibit two single PL peaks with linear polarizations both along the axial direction, which can be accounted for by the Rashba spin–orbit coupling (SOC) effect that can effectively mix the nonemissive Y and bright Z excitons.

RESULTS AND DISCUSSION

Room-Temperature Structural and Optical Characterizations. By means of ligand-regulated reactions at the water–oil interface,[21,22] two batches of $CsPbBr_3$ nanocrystal samples are chemically synthesized with the PL quantum yields as high as ~91% (see Experimental Section). From the transmission electron microscopy image in Figure 1a (Figure 1c) and the statistical histogram in Figure S1a,b (Figure S1c,d), a width of 13.8 ± 2.1 nm (10.9 ± 2.4 nm) and a length of 51.3 ± 7.8 nm (124.0 ± 13.5 nm) can be averagely estimated for the $CsPbBr_3$ nanocrystals contained in the first (second) sample. Because of the obvious length difference, here below we will denote the nanocrystals in the first and second samples as short and long $CsPbBr_3$ NWRs, respectively. As shown in Figure 1b (Figure 1d) from the solution ensemble measurements, the band-edge absorption and PL peaks of the short (long) $CsPbBr_3$ NWRs are located at ~2.402 (~2.433) eV and ~2.386 (~2.395) eV, respectively.

For the optical studies of single $CsPbBr_3$ NWRs, we utilize a picosecond 405 nm laser operated at 5 MHz with a power density of ~1 W/cm^2 (see Experimental Section). As shown in Figure 1e for a single short NWR (SNWR), the PL peak is around ~2.394 eV with a line width of ~85.4 meV. The PL decay curve measured for a single SNWR is plotted in Figure 1f, which can be fitted with a single-exponential lifetime of ~8.62 ns. From the time-dependent measurement shown in Figure 1g, the PL intensity of a single SNWR switches between the high and medium levels drastically with the occasional dropping to a nonemissive level corresponding to nonradiative Auger recombination of charged excitons.[23,24] Although the above PL blinking effect confirms that a single SNWR is being studied, it does not demonstrate the single-photon emission feature from the second-order photon correlation measurement with a large $g^{(2)}(0)$ value of ~0.93 (Figure 1h). Because the $g^{(2)}(0)$ value is proportional to the ratio between the PL quantum yields of biexcitons and of single excitons,[25,26] the above observation suggests that nonradiative Auger recombination of biexcitons[5] is significantly suppressed in a single SNWR due to the weaker quantum confinement as compared to that in 0D QDs. The PL characteristics measured for single long NWRs (LNWRs) are presented in Figure S2, which are similar to those of single SNWRs at room temperature.

Optical Studies of Single $CsPbBr_3$ SNWRs at 4 K. At 4 K, three types of PL spectra can be resolved from the 32 single $CsPbBr_3$ SNWRs studied in our experiment. Fourteen of the single SNWRs exhibit doublet PL peaks with an average energy splitting of ~1.10 meV (Figure 2a) and orthogonally linear polarizations (Figure 2b). Thirteen of the single SNWRs also possess doublet PL peaks but with an average energy splitting of ~2.33 meV (Figure 2c) and parallelly linear polarizations (Figure 2d). For the remaining five of the single SNWRs, two sets of doublet PL peaks are present (Figure 2e,f) with an average central-energy separation of ~11.7 meV. In Figure S4a–f, we provide additional results to show that it is common to observe the above three types of PL spectra from single SNWRs. Statistical histograms for the central-energy and energy-splitting distributions are provided in Figure S5a–c for the single SNWRs emitting one set of doublet PL peaks. We

https://doi.org/10.1021/acs.nanolett.2c00079
Nano Lett. 2022, 22, 2907–2914

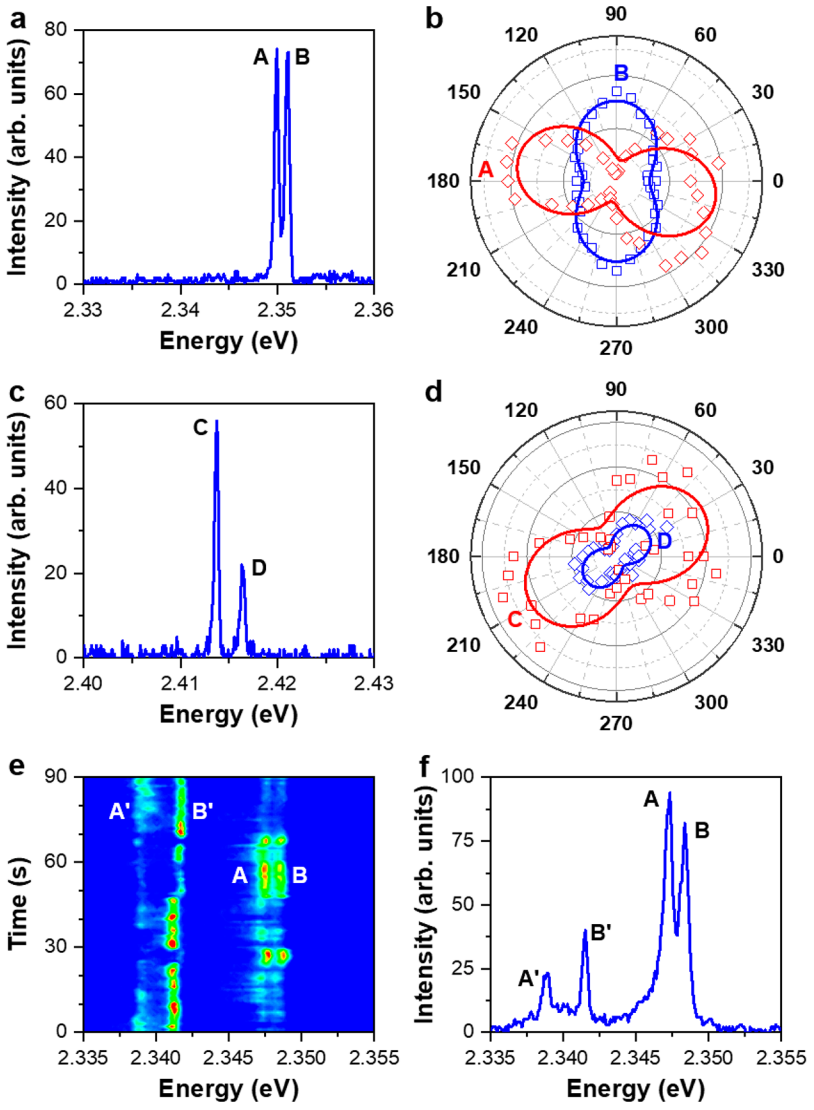

Figure 2. PL spectra and polarization properties of single $CsPbBr_3$ SNWRs at 4 K. (a) PL spectrum measured for a single SNWR with doublet peaks denoted by A and B, respectively. (b) Polar plot showing PL intensities of the A and B peaks of this single SNWR as a function of the detection polarizer angle. See Figure S3a for the PL spectra measured at 0° and 90°, respectively. (c) PL spectrum measured for a single SNWR with doublet peaks denoted by C and D, respectively. (d) Polar plot showing PL intensities of the C and D peaks of this single SNWR as a function of the detection polarizer angle. See Figure S3b for the PL spectra measured at 30° and 120°, respectively. (e) Time-dependent spectral image measured for a single SNWR with anticorrelated PL intensity variations between the lower (denoted by A′ and B′) and higher (denoted by A and B) energy doublet peaks. (f) PL spectrum of this single SNWR extracted from panel e at 51 s.

have also performed second-order photon correlation measurements on the single SNWRs to obtain an average $g^{(2)}(0)$ value of ∼0.51 (see Figure S6), so that they can roughly serve as single-photon emitters at the cryogenic temperature. Moreover, no significant difference is found in the exciton recombination dynamics of the PL peaks such as those shown in Figure 2a,c, which can each be fitted with a single-exponential lifetime of ∼150−300 ps for the single SNWRs studied here or the single LNWRs to be discussed next (see Figure S7).

Optical Studies of Single $CsPbBr_3$ LNWRs at 4 K. The three types of PL spectra mentioned above are similarly observed in the 53 single $CsPbBr_3$ LNWRs studied in our experiment. Thirty of the single LNWRs exhibit doublet PL peaks with an average energy splitting of ∼1.21 meV (Figure 3a) and orthogonally linear polarizations (Figure 3b). Nineteen of the single LNWRs possess doublet PL peaks with an average energy splitting of ∼2.14 meV (Figure 3c) and parallelly linear polarizations (Figure 3d). For the remaining four of the single LNWRs, two sets of doublet PL peaks can be observed with an average central-energy separation of ∼8.9 meV. As can be seen in Figure 3e from the spectral image measured for such a single LNWR, the two sets of doublet PL peaks are quite stable during the measurement time, allowing us to reliably extract their intensity variations as a function of the detection polarizer angle. From the polar plot demonstrated in Figure 3f, the doublet PL peaks contained in either set are orthogonally and linearly polarized, while the higher or lower energy PL peaks taken from both sets have the same linear polarizations. In Figure S8a−f, we provide additional examples for the three types of PL spectra commonly observed in single LNWRs. Statistical histograms for the central-energy and energy-splitting distributions are provided in Figure S5d−f for the single LNWRs emitting one set of doublet PL peaks.

https://doi.org/10.1021/acs.nanolett.2c00079
Nano Lett. 2022, 22, 2907−2914

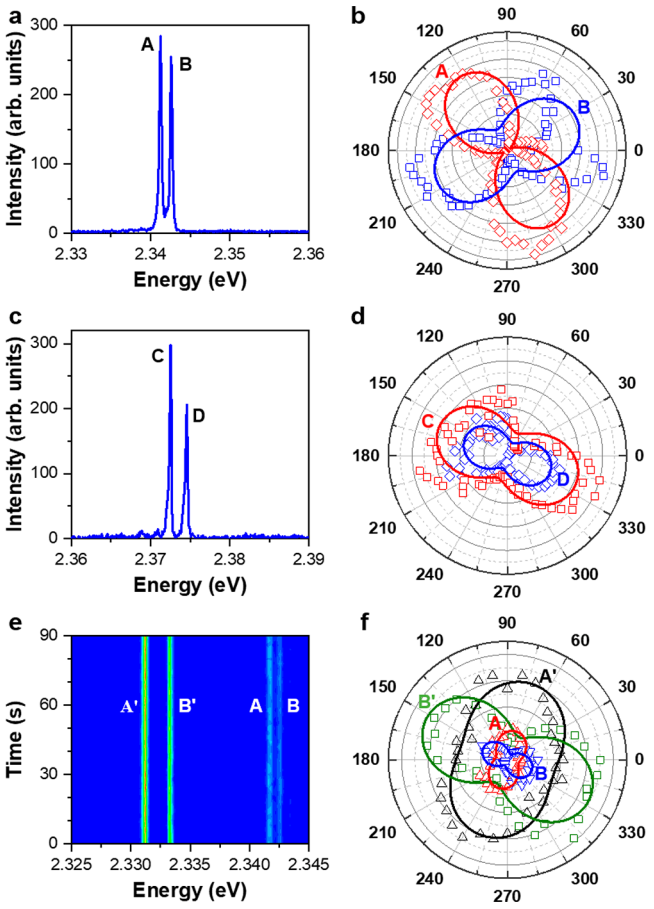

Figure 3. PL spectra and polarization properties of single $CsPbBr_3$ LNWRs at 4 K. (a) PL spectrum measured for a single LNWR with doublet peaks denoted by A and B, respectively. (b) Polar plot showing PL intensities of the A and B peaks of this single LNWR as a function of the detection polarizer angle. See Figure S3c for the PL spectra measured at 120° and 210°, respectively. (c) PL spectrum measured for a single LNWR with doublet peaks denoted by C and D, respectively. (d) Polar plot showing PL intensities of the C and D peaks of this single LNWR as a function of the detection polarizer angle. See Figure S3d for the PL spectra measured at 60° and 150°, respectively. (e) Time-dependent spectral image measured for a single LNWR, where the doublet peaks on the lower (higher) energy side are denoted by A′ and B′ (A and B), respectively. (f) Polar plot showing PL intensities of the A′, B′, A, and B peaks of this single LNWR as a function of the detection polarizer angle.

Although the PL spectra of single LNWRs are similar to those of single SNWRs except an increased stability, the average $g^{(2)}(0)$ value is significantly increased to ~0.95 (see Figure S9), implying that nonradiative Auger interactions among multiple excitons are further reduced due to the more elongated axial length.

Excitation Polarizations of Single $CsPbBr_3$ LNWRs at 4 K. In Figure 4a,b, we provide a spectral image and the associated polar plot measured for a single $CsPbBr_3$ LNWR to show that the doublet PL peaks have orthogonally linear polarizations. Then with unpolarized detection for this single LNWR, we vary the laser linear polarization in Figure 4c,d to demonstrate that the PL intensities of its doublet peaks acquire maximums and minimums synchronously. As shown in Figure 4b, the linear polarization of ~150° (~60°) measured for the lower (higher) energy peak is parallel (perpendicular) to the maximum excitation direction of the linearly polarized laser in Figure 4d. The above observations suggest that after light absorption along the axial direction of a single NWR,[27] the doublet PL states can both be populated by the photogenerated excitons. In Figure 4e,f, we additionally provide a spectral image and the associated polar plot measured for a single LNWR emitting one set of doublet PL peaks with parallelly linear polarizations. Then with unpolarized detection, the laser linear polarization is varied in Figure 4g,h to show that the doublet PL peaks are both linearly polarized along the axial direction. After the linear polarization of each PL peak emitted by a single LNWR has been determined with respect to its axial direction, which can be extended to the SNWR case (see Figure S10), we move on to discuss possible origins for the three types of PL spectra observed in our experiment.

Origins for the Three Types of PL Spectra. If we set the axial direction of a single $CsPbBr_3$ NWR along the z-axis, according to previous optical studies of single perovskite QDs,[28−30] the energy-level structure of band-edge excitons is composed of in-plane X and Y orthogonal states, out-of-plane Z state, and dark D state (see theoretical discussions in the Supporting Information). Although the X, Y, and Z states should be all emissive due to their bright-exciton feature, it was quite common to observe only doublet PL peaks from a single perovskite QD with orthogonally linear polarizations.[28−30] The missing bright-exciton state might have the highest energy to prevent its thermal population, a weak oscillator strength or an emission dipole parallel to the PL collection axis.[30−32] For the single NWRs studied here with a flat-lying configuration on the sample substrate (Figure 1a,c), the emission dipoles of X/Y and Z excitons should be distributed within the cross-sectional plane and along the axial direction, respectively.[33,34] Because of the strong anisotropy of depolarization field in a single NWR,[2] luminescence polarized along the long axis (Z-state) is strong whereas the electric fields of light within the cross-sectional plane (X and Y states) are reduced by $2\varepsilon/(\varepsilon + \varepsilon_{NWR})$ with ε and ε_{NWR} being dielectric constants of the environment and the NWR, respectively.

When assuming that our PL collection is along the y-axis, the Y exciton would be nonemissive since its electric field is also polarized along the same direction. This explains the first type of PL spectrum observed in our experiment from single NWRs (Figure 2a,b and Figure 3a,b), wherein the higher and lower energy ones of the doublet PL peaks should be contributed by the X and Z excitons whose linear polarizations are parallel to the x- and z-axes, respectively. As for the second type of PL spectrum consisting of doublet PL peaks with parallelly linear polarizations (Figure 2c,d and Figure 3c,d), we notice that in a noncentrosymmetric NWR the Rashba effects in the conduction and valence bands can give rise to a SOC between the exciton's center-of-mass momentum and spin, which would in turn mix the bright Z and the "dark" Y excitons (see theoretical discussions in the Supporting Information). This SOC-induced mixing would spread the strong oscillator strength of the Z exciton into the Y exciton, making the latter one visible to our PL collection with a linear polarization parallel to the z axis. The absent emission of X exciton in this case might be caused by its low population. It was postulated previously that the Rashba effect could be triggered in 0D perovskite QDs to place the dark-exciton state higher in energy than those of the bright-exciton states.[30] As revealed from recent magneto-optical studies of single perovskite QDs,[34,35] the lowest exciton state is in fact dark and the exciton fine structures should be determined mainly by the electron−hole

https://doi.org/10.1021/acs.nanolett.2c00079
Nano Lett. 2022, 22, 2907−2914

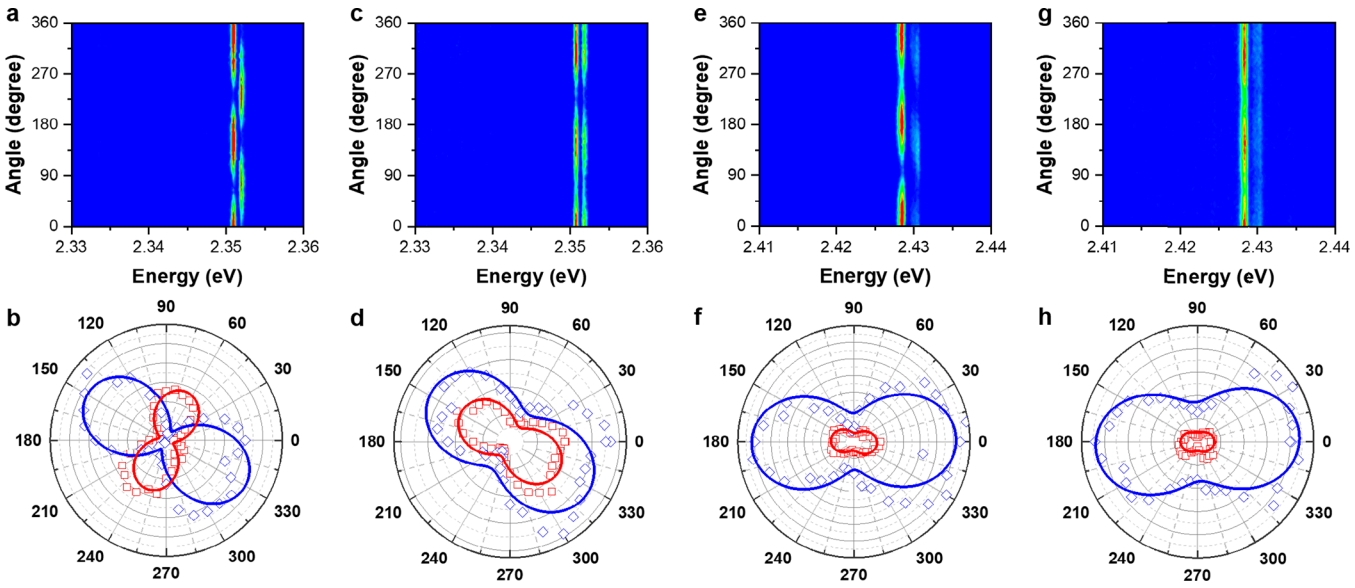

Figure 4. Excitation polarizations of single $CsPbBr_3$ LNWRs at 4 K. (a) PL spectral image and (b) the associated polar plot measured for a single LNWR, showing anticorrelated intensity variations of the doublet PL peaks with the detection polarizer angles. (c) PL spectral image and (d) the associated polar plot measured for this single LNWR, showing synchronous intensity variations of the doublet PL peaks with the linear polarization angles of the excitation laser. (e) PL spectral image and (f) the associated polar plot measured for a single LNWR, showing synchronous intensity variations of the doublet PL peaks with the detection polarizer angles. (g) PL spectral image and (h) the associated polar plot measured for this single LNWR, showing synchronous intensity variations of the doublet PL peaks with the linear polarization angles of the excitation laser. In panels b, d, f, or h, the blue (red) data points and fitted lines correspond to the lower (higher) energy peak of the PL doublet emitted by a single LNWR.

exchange interaction instead of the Rashba effect. Nevertheless, the Rashba effect could be still important in the perovskite nanostructures with weak quantum confinement,[36] such as the single NWRs studied here. In particular, our measurements indicate that the Rashba effect can manifest itself in the polarization patterns of PL peaks in perovskite NWRs.

Compared to the first and second types of PL spectra discussed above, the third type is most intriguing as it is contributed by two sets of doublet PL peaks each with orthogonally linear polarizations (Figure 2e,f and Figure 3e,f). The central-energy separation between the two sets (~9−12 meV) is much greater than the exciton fine-structure splitting due to long- and short-range exchanges (<0.5$\hbar\omega_{LT}$, ~3 meV)[37] and it is also significantly smaller than the energy separation between the first (1s) and second (2s) exciton excited states with a value of 0.75E_b (~30 meV).[38] As such, both the fine structure (spin) and relative electron−hole motion of excitons can be safely ruled out as the sources for the two sets of doublet PL peaks. We note, however, the exciton should have another degree of freedom dictated by the center-of-mass motion of its composing electron and hole. Since the dimensions of $CsPbBr_3$ NWRs synthesized by us are larger than the exciton Bohr diameter of ~7 nm,[39] the relative motion of electron and hole is little influenced by the quantum-confinement effect. However, the exciton's center-of-mass motion within the cross-sectional plane of the NWRs becomes quantized, just as the motion of an electron or a hole would be. In the x−y plane perpendicular to the NWR axis, the center-of-mass momentum for the X or Y exciton can be written as $K_{x,y} = n\pi/L_{x,y}$ (n = 1, 2, . . .) with $L_{x,y}$ being the NWR dimension along the x- or y-axis. The recombination energy of X or Y exciton would be likewise quantized with the neighboring splitting being proportional to $\frac{h^2}{ML_{x,y}^2}$, where h is the Planck constant and M is the exciton's mass. The lower- and higher-energy doublet PL peaks should correspond to the X and Z excitons recombining from the first and second excited states, respectively, with the center-of-mass quantized motions. According to our theoretical calculations detailed in the Supporting Information, the estimated energy separation between these quantized center-of-mass states matches well with that extracted from our experiment for the two sets of doublet PL peaks.

On the basis of the observation that two sets of doublet PL peaks can be simultaneously detected, we speculate that the relaxation process between the quantized center-of-mass states should be slow (see Figure S11 for the PL decay measurements), which might be caused by the mismatch between their central-energy separation and the optical phonon energy. As can be seen from Figure S12 for a representative single LNWR, the lower-energy doublet peaks get saturated at higher laser power densities with the accompanied intensity increase of the higher-energy ones. This band-filling effect further confirms that there does exist an exciton relaxation process from the second to the first quantized center-of-mass states. Moreover, the exciton−phonon coupling strength of low-dimensional perovskites is positively correlated with the degree of quantum-confinement,[40] implying that the weak quantum confinement in single $CsPbBr_3$ NWRs with reduced exciton−phonon coupling could serve as another important factor to make the exciton relaxation process inefficient.[41] This is consistent with the fact that the optical phonon replicas can be readily observed in previous optical studies of single $CsPbBr_3$ QDs,[34] while they are completely missing in the single $CsPbBr_3$ NWRs studied here (see Figure 2a,c and Figure 3a,c). As such, the anticorrelated intensity variations of the two sets of doublet PL peaks in Figure 2e strongly suggests that there exists a dynamic relaxation channel connecting the higher- and lower-energy doublet peaks, which renders the higher-energy doublet peaks sometimes nonemissive. Compared to single LNWRs, the

https://doi.org/10.1021/acs.nanolett.2c00079
Nano Lett. 2022, 22, 2907−2914

single SNWRs possess a larger surface-to-volume ratio to make them more vulnerable to environmental charge fluctuations, which could affect the crystal structure and the strength of exciton−phonon coupling.[42−44]

CONCLUSION

To summarize, we have synthesized perovskite $CsPbBr_3$ NWRs, whose emission energies (see Figure S5a,d) are located between those of 0D $CsPbBr_3$ QDs[28] and bulk $CsPbBr_3$ crystals,[45] and characterized their single-particle optical properties mainly at 4 K. Compared to perovskite NWRs studied previously with much larger dimensions,[46−48] the $CsPbBr_3$ NWRs focused here fall within the weak quantum-confinement regime, which allows us to reveal novel quantum-optical and atomic-like photophysics of this important 1D material. Consistent with the 0D QDs, a single NWR can emit one set of doublet PL peaks from the *X* and *Z* excitons with orthogonally linear polarizations, and their energy splitting of several millielectronvolts is caused primarily by the long-range exchange interaction. One set of doublet PL peaks with parallelly linear polarizations can also be observed from some other single NWRs, suggesting an effective mixing of the *Y* and *Z* excitons via the Rashba effect. Interestingly, two sets of doublet PL peaks can also be observed from a single NWR with a central-energy separation of ∼10 meV, which is attributed to the quantized center-of-mass motion of excitons perpendicular to the axial direction (see Supporting Information for a unified description of the three types of PL spectra). The above findings have thus provided a comprehensive view on the intrinsic energy-level structures and recombination dynamics of excitons in 1D semiconductor nanostructures. These single NWRs can then serve as an ideal platform for further explorations of fascinating 1D photophysics, thus complementing their well-studied 2D[32,49,50] and 0D[20,28−31,34,35] counterparts in terms of both fundamental studies and practical applications.

EXPERIMENTAL SECTION

Chemical Synthesis of $CsPbBr_3$ NWRs. The $CsPbBr_3$ NWRs are chemically transformed from Cs_4PbBr_6 nanopolyhedrons at the water−oil interface with the assistance of ligand regulation.[21,22] To prepare Cs_4PbBr_6 nanopolyhedrons, 1 mL of oleylamine (OAm), 1 mL of oleic acid (OA), 10 mL of 1-octadecene (ODE), and 0.2 mmol of $PbBr_2$ are first loaded into a 50 mL three-neck flask. The mixture is degassed next for 0.5 h at 120 °C, and then heated to 150 °C under the N_2 flow. A 4.4 mL sample of Cs-oleate solution (prepared by dissolving 0.16 g of Cs_2CO_3 in 16 mL of ODE and 1 mL of OA) is injected rapidly into the above $PbBr_2$ solution, and the reaction is stopped after 10 s with an ice−water bath. With a volume ratio of 1:1, acetone is added to the above solution to precipitate Cs_4PbBr_6 nanopolyhedrons. The product is centrifuged next at 8000 rpm for 3 min, after which the supernatant is discarded and the precipitate is redispersed in 10 mL of cyclohexane.

To prepare the $CsPbBr_3$ NWRs, 4 mL of the Cs_4PbBr_6 nanopolyhedrons solution is contained inside a 15 mL centrifuge tube to which different amounts of tetraoctylammonium bromide (TOAB) solution (0.01 M dissolved in 3 mL of toluene) are added. After 0.2 mL of water is injected, the mixture is shaken vigorously for 20 s to form the desired $CsPbBr_3$ NWRs. The length of the $CsPbBr_3$ NWRs is tuned by the added amounts of TOAB solution, which are typically 10 and 30 μL for the formation of $CsPbBr_3$ SNWRs and LNWRs, respectively. Without the addition of TOAB solution, the Cs_4PbBr_6 nanopolyhedrons are simply transformed into the $CsPbBr_3$ nanocubes at the water−oil interface featuring an almost symmetric cross section.[21]

Optical Measurements. One drop of the diluted solution of colloidal $CsPbBr_3$ NWRs is spin-coated onto a fused silica substrate to form a solid film for the single-particle optical characterizations. The sample substrate is attached to the coldfinger of a helium-free cryostat operated at either room or 4 K temperature. The output beam from a 405 nm picosecond diode laser operated at a repetition rate of 5 MHz is focused onto the sample substrate by a dry objective with a numerical aperture of 0.82. Unless otherwise specified in the text, the laser power density of ∼1 W/cm^2 is utilized to set $\langle N\rangle = 0.1$ for a single $CsPbBr_3$ NWR with $\langle N\rangle$ being the number of excitons generated per pulse in a single $CsPbBr_3$ QD with a similar edge width.[20] The PL signal of a single NWR is collected by the same objective and sent through a 0.5 m spectrometer to a CCD camera for the PL spectral measurement with an integration time of 1 s. The PL signal of a single NWR can be alternatively sent through a nonpolarizing 50/50 beam splitter to two avalanche photodiodes for the PL decay and second-order photon correlation measurements with a time resolution of ∼100 ps. Whenever it is necessary, a half waveplate and a linear polarizer would be added to the optical path for the polarization-dependent optical measurements.

ASSOCIATED CONTENT

Supporting Information

The Supporting Information is available free of charge at https://pubs.acs.org/doi/10.1021/acs.nanolett.2c00079.

Theoretical calculations, statistical histograms for the width and length distributions of single LNWRs and SNWRs, room-temperature optical properties of single LNWRs, 4 K PL spectra measured at different polarization angles for single LNWRs and SNWRs, three types of PL spectra measured for single LNWRs and SNWRs at 4 K, statistical histograms of the central-energy and energy-splitting distributions extracted at 4 K for the doublet PL peaks emitted from single LNWRs and SNWRs, second-order photon correlation measurements on single LNWRs and SNWRs at 4 K, excitation polarizations measured at 4 K for single SNWRs, PL decay curves measured for single SNWRs and LNWRs at 4 K, and 4 K PL spectra measured for a single LNWR at different laser power densities (PDF)

AUTHOR INFORMATION

Corresponding Authors

Zhi-Gang Yu − *Sivananthan Laboratories, Bolingbrook, Illinois 60440, United States; Department of Physics and Astronomy, Washington State University, Pullman, Washington 99164, United States;* orcid.org/0000-0002-1376-9025; Email: zhi-gang.yu@wsu.edu

Zhenda Lu − *College of Engineering and Applied Sciences, Nanjing University, Nanjing 210093, China;* orcid.org/0000-0002-9616-8814; Email: luzhenda@nju.edu.cn

Min Xiao − *National Laboratory of Solid State Microstructures, School of Physics, and Collaborative Innovation Center of Advanced Microstructures, Nanjing*

https://doi.org/10.1021/acs.nanolett.2c00079
Nano Lett. 2022, 22, 2907−2914

University, Nanjing 210093, China; Department of Physics, University of Arkansas, Fayetteville, Arkansas 72701, United States; Email: mxiao@uark.edu

Xiaoyong Wang − *National Laboratory of Solid State Microstructures, School of Physics, and Collaborative Innovation Center of Advanced Microstructures, Nanjing University, Nanjing 210093, China*; orcid.org/0000-0003-1147-0051; Email: wxiaoyong@nju.edu.cn

Authors

Ying Tang − *National Laboratory of Solid State Microstructures, School of Physics, and Collaborative Innovation Center of Advanced Microstructures, Nanjing University, Nanjing 210093, China*

Chunyang Yin − *National Laboratory of Solid State Microstructures, School of Physics, and Collaborative Innovation Center of Advanced Microstructures, Nanjing University, Nanjing 210093, China*

Qiang Jing − *College of Engineering and Applied Sciences, Nanjing University, Nanjing 210093, China*

Chunfeng Zhang − *National Laboratory of Solid State Microstructures, School of Physics, and Collaborative Innovation Center of Advanced Microstructures, Nanjing University, Nanjing 210093, China*; orcid.org/0000-0001-9030-5606

Complete contact information is available at: https://pubs.acs.org/10.1021/acs.nanolett.2c00079

Author Contributions

#Y.T., C.Y., and Q.J. contributed equally to this work.

Notes

The authors declare no competing financial interest.

■ ACKNOWLEDGMENTS

This work is supported by the National Key Research and Development Program of China (No. 2021YFA1400802, No. 2019YFA0308700, and No. 2017YFA0303700), the National Natural Science Foundation of China (No. 62174081 and No. 61974058), and the Priority Academic Program Development of Jiangsu Higher Education Institutions.

■ REFERENCES

(1) Li, Y.; Qian, F.; Xiang, J.; Lieber, C. M. Nanowire Electronic and Optoelectronic Devices. *Mater. Today* **2006**, *9*, 18−27.

(2) Shabaev, A.; Efros, A. L. 1D Exciton Spectroscopy of Semiconductor Nanorods. *Nano Lett.* **2004**, *4*, 1821−1825.

(3) Hu, J.; Li, L.-S.; Yang, W.; Manna, L.; Wang, L.-W.; Alivisatos, A. P. Linearly Polarized Emission from Colloidal Semiconductor Quantum Rods. *Science* **2001**, *292*, 2060−2063.

(4) Le Thomas, N.; Herz, E.; Schops, O.; Woggon, U.; Artemyev, M. V. Exciton Fine Structure in Single CdSe Nanorods. *Phys. Rev. Lett.* **2005**, *94*, 016803.

(5) Htoon, H.; Hollingsworth, J. A.; Dickerson, R.; Klimov, V. I. Effect of Zero- to One-Dimensional Transformation on Multiparticle Auger Recombination in Semiconductor Quantum Rods. *Phys. Rev. Lett.* **2003**, *91*, 227401.

(6) Rothenberg, E.; Kazes, M.; Shaviv, E.; Banin, U. Electric Field Induced Switching of the Fluorescence of Single Semiconductor Quantum Rods. *Nano Lett.* **2005**, *5*, 1581−1586.

(7) Vietmeyer, F.; Frantsuzov, P. A.; Janko, B.; Kuno, M. Carrier Recombination Dynamics in Individual CdSe Nanowires. *Phys. Rev. B* **2011**, *83*, 115319.

(8) Glennon, J. J.; Tang, R.; Buhro, W. E.; Loomis, R. A. Synchronous Photoluminescence Intermittency (Blinking) along Whole Semiconductor Quantum Wires. *Nano Lett.* **2007**, *7*, 3290−3295.

(9) Protasenko, V. V.; Hull, K. L.; Kuno, M. Disorder-Induced Optical Heterogeneity in Single CdSe Nanowires. *Adv. Mater.* **2005**, *17*, 2942−2949.

(10) Schäfer, S.; Wang, Z.; Zierold, R.; Kipp, T.; Mews, A. Laser-Induced Charge Separation in CdSe Nanowires. *Nano Lett.* **2011**, *11*, 2672−2677.

(11) Htoon, H.; O'Connell, M. J.; Cox, P. J.; Doorn, S. K.; Klimov, V. I. Low Temperature Emission Spectra of Individual Single-Walled Carbon Nanotubes: Multiplicity of Subspecies within Single-Species Nanotube Ensembles. *Phys. Rev. Lett.* **2004**, *93*, 027401.

(12) Carlson, L. J.; Maccagnano, S. E.; Zheng, M.; Silcox, J.; Krauss, T. D. Fluorescence Efficiency of Individual Carbon Nanotubes. *Nano Lett.* **2007**, *7*, 3698−3703.

(13) Ma, Y.-Z.; Valkunas, L.; Dexheimer, S. L.; Bachilo, S. M.; Fleming, G. R. Femtosecond Spectroscopy of Optical Excitations in Single-Walled Carbon Nanotubes: Evidence for Exciton-Exciton Annihilation. *Phys. Rev. Lett.* **2005**, *94*, 157402.

(14) Murakami, Y.; Kono, J. Nonlinear Photoluminescence Excitation Spectroscopy of Carbon Nanotubes: Exploring the Upper Density Limit of One-Dimensional Excitons. *Phys. Rev. Lett.* **2009**, *102*, 037401.

(15) He, X.; Htoon, H.; Doorn, S. K.; Pernice, W. H. P.; Pyatkov, F.; Krupke, R.; Jeantet, A.; Chassagneux, Y.; Voisin, C. Carbon Nanotubes as Emerging Quantum-Light Sources. *Nat. Mater.* **2018**, *17*, 663−670.

(16) Hofmann, M. S.; Glückert, J. T.; Noé, J.; Bourjau, C.; Dehmel, R.; Högele, A. Bright, Long-Lived and Coherent Excitons in Carbon Nanotube Quantum Dots. *Nat. Nanotechnol.* **2013**, *8*, 502−505.

(17) Ghosh, S.; Bachilo, S. M.; Simonette, R. A.; Beckingham, K. M.; Weisman, R. B. Oxygen Doping Modifies Near-Infrared Band Gaps in Fluorescent Single-Walled Carbon Nanotubes. *Science* **2010**, *330*, 1656−1659.

(18) Piao, Y.; Meany, B.; Powell, L. R.; Valley, N.; Kwon, H.; Schatz, G. C.; Wang, Y. H. Brightening of Carbon Nanotube Photoluminescence through the Incorporation of Sp^3 Defects. *Nat. Chem.* **2013**, *5*, 840−845.

(19) Akkerman, Q. A.; Raino, G.; Kovalenko, M. V.; Manna, L. Genesis, Challenges and Opportunities for Colloidal Lead Halide Perovskite Nanocrystals. *Nat. Mater.* **2018**, *17*, 394−405.

(20) Hu, F.; Zhang, H.; Sun, C.; Yin, C.; Lv, B.; Zhang, C.; Yu, W. W.; Wang, X.; Zhang, Y.; Xiao, M. Superior Optical Properties of Perovskite Nanocrystals as Single Photon Emitters. *ACS Nano* **2015**, *9*, 12410−12416.

(21) Jing, Q.; Su, Y.; Xing, X.; Lu, Z. Highly Luminescent $CsPbBr_3$ Nanorods Synthesized by a Ligand-Regulated Reaction at the Water-Oil Interface. *J. Mater. Chem. C* **2019**, *7*, 1854−1858.

(22) Wu, L.; Hu, H.; Xu, Y.; Jiang, S.; Chen, M.; Zhong, Q.; Yang, D.; Liu, Q.; Zhao, Y.; Sun, B.; Zhang, Q.; Yin, Y. From Nonluminescent Cs_4PbX_6 (X = Cl, Br, I) Nanocrystals to Highly Luminescent $CsPbX_3$ Nanocrystals: Water-Triggered Transformation through a CsX-Stripping Mechanism. *Nano Lett.* **2017**, *17*, 5799−5804.

(23) Galland, C.; Ghosh, Y.; Steinbrück, A.; Sykora, M.; Hollingsworth, J. A.; Klimov, V. I.; Htoon, H. Two Types of Luminescence Blinking Revealed by Spectroelectrochemistry of Single Quantum Dots. *Nature* **2011**, *479*, 203−207.

(24) Hu, F.; Yin, C.; Zhang, H.; Sun, C.; Yu, W. W.; Zhang, C.; Wang, X.; Zhang, Y.; Xiao, M. Slow Auger Recombination of Charged Excitons in Nonblinking Perovskite Nanocrystals without Spectral Diffusion. *Nano Lett.* **2016**, *16*, 6425−6430.

(25) Nair, G.; Zhao, J.; Bawendi, M. G. Biexciton Quantum Yield of Single Semiconductor Nanocrystals from Photon Statistics. *Nano Lett.* **2011**, *11*, 1136−1140.

(26) Park, Y.-S.; Malko, A. V.; Vela, J.; Chen, Y.; Ghosh, Y.; García-Santamaría, F.; Hollingsworth, J. A.; Klimov, V. I.; Htoon, H. Near-Unity Quantum Yields of Biexciton Emission from CdSe/CdS

Nanocrystals Measured Using Single-Particle Spectroscopy. *Phys. Rev. Lett.* **2011**, *106*, 187401.
(27) Kim, H.; Kim, I.; Kyhm, K.; Taylor, R. A.; Kim, J. S.; Song, J. D.; Je, K. C.; Dang, L. S. Exciton Dipole-Dipole Interaction in a Single Coupled-Quantum-Dot Structure *via* Polarized Excitation. *Nano Lett.* **2016**, *16*, 7755−7760.
(28) Fu, M.; Tamarat, P.; Huang, H.; Even, J.; Rogach, A. L.; Lounis, B. Neutral and Charged Exciton Fine Structure in Single Lead Halide Perovskite Nanocrystals Revealed by Magneto-Optical Spectroscopy. *Nano Lett.* **2017**, *17*, 2895−2901.
(29) Yin, C.; Chen, L.; Song, N.; Lv, Y.; Hu, F.; Sun, C.; Yu, W. W.; Zhang, C.; Wang, X.; Zhang, Y.; Xiao, M. Bright-Exciton Fine-Structure Splittings in Single Perovskite Nanocrystals. *Phys. Rev. Lett.* **2017**, *119*, 026401.
(30) Becker, M. A.; Vaxenburg, R.; Nedelcu, G.; Sercel, P. C.; Shabaev, A.; Mehl, M. J.; Michopoulos, J. G.; Lambrakos, S. G.; Bernstein, N.; Lyons, J. L.; Stoferle, T.; Mahrt, R. F.; Kovalenko, M. V.; Norris, D. J.; Raino, G.; Efros, A. L. Bright Triplet Excitons in Caesium Lead Halide Perovskites. *Nature* **2018**, *553*, 189−193.
(31) Yin, C.; Lv, Y.; Zhang, X.; Zhang, Y.; Yu, W. W.; Zhang, C.; Yu, Z.-G.; Wang, X.; Xiao, M. Transition from Doublet to Triplet Excitons in Single Perovskite Nanocrystals. *J. Phys. Chem. Lett.* **2020**, *11*, 5750−5755.
(32) Schmitz, A.; Montanarella, F.; Schaberg, L. L.; Abdelbaky, M.; Kovalenko, M. V.; Bacher, G. Optical Probing of Crystal Lattice Configurations in Single $CsPbBr_3$ Nanoplatelets. *Nano Lett.* **2021**, *21*, 9085−9092.
(33) Folie, B. D.; Tan, J. A.; Huang, J.; Sercel, P. C.; Delor, M.; Lai, M.; Lyons, J. L.; Bernstein, N.; Efros, A. L.; Yang, P.; Ginsberg, N. S. Effect of Anisotropic Confinement on Electronic Structure and Dynamics of Band Edge Excitons in Inorganic Perovskite Nanowires. *J. Phys. Chem. A* **2020**, *124*, 1867−1876.
(34) Tamarat, P.; Hou, L.; Trebbia, J.-B.; Swarnkar, A.; Biadala, L.; Louyer, Y.; Bodnarchuk, M. I.; Kovalenko, M. V.; Even, J.; Lounis, B. The Dark Exciton Ground State Promotes Photon-Pair Emission in Individual Perovskite Nanocrystals. *Nat. Commun.* **2020**, *11*, 6001.
(35) Tamarat, P.; Bodnarchuk, M. I.; Trebbia, J.-B.; Erni, R.; Kovalenko, M. V.; Even, J.; Lounis, B. The Ground Exciton State of Formamidinium Lead Bromide Perovskite Nanocrystals is a Singlet Dark State. *Nat. Mater.* **2019**, *18*, 717−724.
(36) Sercel, P. C.; Lyons, J. L.; Wickramaratne, D.; Vaxenburg, R.; Bernstein, N.; Efros, A. L. Exciton Fine Structure in Perovskite Nanocrystals. *Nano Lett.* **2019**, *19*, 4068−4077.
(37) Nestoklon, M. O.; Goupalov, S. V.; Dzhioev, R. I.; Ken, O. S.; Korenev, V. L.; Kusrayev, Yu. G.; Sapega, V. F.; de Weerd, C.; Gomez, L.; Gregorkiewicz, T.; Lin, J.; Suenaga, K.; Fujiwara, Y.; Matyushkin, L. B.; Yassievich, I. N. Optical Orientation and Alignment of Excitons in Ensembles of Inorganic Perovskite Nanocrystals. *Phys. Rev. B* **2018**, *97*, 235304.
(38) Ai, B.; Liu, C.; Deng, Z.; Wang, J.; Han, J.; Zhao, X. Low Temperature Photoluminescence Properties of $CsPbBr_3$ Quantum Dots Embedded in Glasses. *Phys. Chem. Chem. Phys.* **2017**, *19*, 17349−17355.
(39) Protesescu, L.; Yakunin, S.; Bodnarchuk, M. I.; Krieg, F.; Caputo, R.; Hendon, C. H.; Yang, R. X.; Walsh, A.; Kovalenko, M. V. Nanocrystals of Cesium Lead Halide Perovskites ($CsPbX_3$, X = Cl, Br, and I): Novel Optoelectronic Materials Showing Bright Emission with Wide Color Gamut. *Nano Lett.* **2015**, *15*, 3692−3696.
(40) Cho, K.; Yamada, T.; Tahara, H.; Tadano, T.; Suzuura, H.; Saruyama, M.; Sato, R.; Teranishi, T.; Kanemitsu, Y. Luminescence Fine Structures in Single Lead Halide Perovskite Nanocrystals: Size Dependence of the Exciton−Phonon Coupling. *Nano Lett.* **2021**, *21*, 7206−7212.
(41) Kennehan, E. R.; Doucette, G. S.; Marshall, A. R.; Grieco, C.; Munson, K. T.; Beard, M. C.; Asbury, J. B. Electron-Phonon Coupling and Resonant Relaxation from 1D and 1P States in PbS Quantum Dots. *ACS Nano* **2018**, *12*, 6263−6272.
(42) Guzelturk, B.; Winkler, T.; Van de Goor, T. W. J.; Smith, M. D.; Bourelle, S. A.; Feldmann, S.; Trigo, M.; Teitelbaum, S. W.; Steinrück, H.-G.; de la Pena, G. A.; Alonso-Mori, R.; Zhu, D.; Sato, T.; Karunadasa, H. I.; Toney, M. F.; Deschler, F.; Lindenberg, A. M. Visualization of Dynamic Polaronic Strain Fields in Hybrid Lead Halide Perovskites. *Nat. Mater.* **2021**, *20*, 618−623.
(43) Cannelli, O.; Colonna, N.; Puppin, M.; Rossi, T. C.; Kinschel, D.; Leroy, L. M. D.; Löffler, J.; Budarz, J. M.; March, A. M.; Doumy, G.; Al Haddad, A.; Tu, M.-F.; Kumagai, Y.; Walko, D.; Smolentsev, G.; Krieg, F.; Boehme, S. C.; Kovalenko, M. V.; Chergui, M.; Mancini, G. F. Quantifying Photoinduced Polaronic Distortions in Inorganic Lead Halide Perovskite Nanocrystals. *J. Am. Chem. Soc.* **2021**, *143*, 9048−9059.
(44) Kennehan, E. R.; Munson, K. T.; Grieco, C.; Doucette, G. S.; Marshall, A. R.; Beard, M. C.; Asbury, J. B. Exciton-Phonon Coupling and Carrier Relaxation in PbS Quantum Dots: The Case of Carboxylate Ligands. *J. Phys. Chem. C* **2021**, *125*, 22622−22629.
(45) Belykh, V. V.; Yakovlev, D. R.; Glazov, M. M.; Grigoryev, P. S.; Hussain, M.; Rautert, J.; Dirin, D. N.; Kovalenko, M. V.; Bayer, M. Coherent Spin Dynamics of Electrons and Holes in $CsPbBr_3$ Perovskite Crystals. *Nat. Commun.* **2019**, *10*, 673.
(46) Zhu, H.; Fu, Y.; Meng, F.; Wu, X.; Gong, Z.; Ding, Q.; Gustafsson, M. V.; Trinh, M. T.; Jin, S.; Zhu, X.-Y. Lead Halide Perovskite Nanowire Lasers with Low Lasing Thresholds and High Quality Factors. *Nat. Mater.* **2015**, *14*, 636−642.
(47) Fu, Y.; Zhu, H.; Stoumpos, C. C.; Ding, Q.; Wang, J.; Kanatzidis, M. G.; Zhu, X.; Jin, S. Broad Wavelength Tunable Robust Lasing from Single-Crystal Nanowires of Cesium Lead Halide Perovskites ($CsPbX_3$, X = Cl, Br, I). *ACS Nano* **2016**, *10*, 7963−7972.
(48) Shang, Q.; Zhang, S.; Liu, Z.; Chen, J.; Yang, P.; Li, C.; Li, W.; Zhang, Y.; Xiong, Q.; Liu, X.; Zhang, Q. Surface Plasmon Enhanced Strong Exciton-Photon Coupling in Hybrid Inorganic-Organic Perovskite Nanowires. *Nano Lett.* **2018**, *18*, 3335−3343.
(49) Do, T. T. H.; Del Águila, A. G.; Zhang, D.; Xing, J.; Liu, S.; Prosnikov, M. A.; Gao, W.; Chang, K.; Christianen, P. C. M.; Xiong, Q. Bright Exciton Fine-Structure in Two-Dimensional Lead Halide Perovskites. *Nano Lett.* **2020**, *20*, 5141−5148.
(50) Huo, C.; Fong, C. F.; Amara, M.-R.; Huang, Y.; Chen, B.; Zhang, H.; Guo, L.; Li, H.; Huang, W.; Diederichs, C.; Xiong, Q. Optical Spectroscopy of Single Colloidal $CsPbBr_3$ Perovskite Nanoplatelets. *Nano Lett.* **2020**, *20*, 3673−3680.

https://doi.org/10.1021/acs.nanolett.2c00079
Nano Lett. 2022, 22, 2907−2914